Materials and Structures (2007) 40:813–825
DOI 10.1617/s11527-007-9243-z

ORIGINAL ARTICLE

Drying induced moisture losses from mortar to the environment. Part II: numerical implementation

M. Azenha · K. Maekawa · T. Ishida · R. Faria

Received: 3 March 2006 / Accepted: 20 March 2007 / Published online: 4 May 2007

Abstract This paper presents a novel methodology to appropriately account for boundary conditions in numerical analyses of moisture fields in cementitious materials. The proposed methodology consists of using experimentally obtained moisture emissivity coefficients together with the vapour pressure difference between the environment and the exposed surface (based on the average surface humidity content). The performance of such methodology (implemented on DuCOM, a computational code suitable for calculation of moisture/temperature fields in cementitious materials) is evaluated by comparing the numerical predictions with the experimental results presented in the Part I companion paper. Influences of the many environmental conditions reported in Part I are investigated for validation of the proposed numerical methodology: temperature, relative humidity, wind speed and age of exposure of specimens. Furthermore, an additional numerical formulation for inclusion of the effect of evaporative cooling, based on the computation of additional heat fluxes induced by evaporative moisture losses, is presented, together with a validation example. Finally, two numerical sensitivity analyses are put forward for clarification of the relative importance of the parameters involved in moisture loss from cementitious materials, as well as the relevance of the evaporative cooling.

Résumé *Cet article présente une nouvelle méthodologie afin de mieux tenir compte des conditions limites lors d'analyses numériques des champs d'humidité dans les matériaux cimentaires. La méthodologie proposée consiste à utiliser des coefficients d'émissivité d'humidité obtenus expérimentalement associés avec la différence de pression de vapeur entre l'environnement extérieur et la surface exposée du béton (basée sur le contenu moyen de l'humidité à la surface). La validité de cette méthodologie (intégrée dans un logiciel de calcul des champs d'humidité et de température des matériaux cimentaires—appelé DuCOM) est évaluée en comparant les prédictions aux résultats expérimentaux rapportés dans l'article précédant (partie 1). Les influences des nombreuses conditions environnementales rapportées dans la partie 1 y sont vérifiées et validées, notamment: la température, l'humidité relative, la vitesse du vent et la durée d'exposition des spécimens. En*

M. Azenha · R. Faria
Faculty of Engineering, University of Porto, Porto, Portugal

K. Maekawa · T. Ishida
School of Engineering, University of Tokyo, Tokyo, Japan

M. Azenha (✉)
Civil Engineering Department, Faculty of Engineering of the University of Porto, R. Dr. Roberto Frias, s/n - 4200-465 Porto, Portugal
e-mail: mazenha@fe.up.pt

outre, une formulation numérique additionnelle pour inclure l'effet du refroidissement par évaporation (basée sur le calcul des flux de chaleur additionnels induits par évaporation) est présentée et validée avec un exemple. En conclusion, deux analyses de sensibilité sont présentées pour clarifier l'importance relative des paramètres impliqués dans la perte d'humidité des matériaux cimentaires et pour démontrer la pertinence de l'influence du refroidissement par évaporation.

Keywords Cement · Moisture · Evaporation · Evaporative cooling · Numerical simulation · Boundary conditions

1 Introduction

1.1 Overview

In the companion paper concerned with Part I [1] an experimental campaign was presented, with the aim of better understanding the moisture losses from hardening cementitious materials to the environment.

In this paper a novel formulation for numerical simulation of moisture boundary conditions will be presented. Such formulation was implemented in an existing computational framework named DuCOM, which has been under development in the University of Tokyo [2, 3]. This framework comprises multi-scale finite element modelling (with integration in the time domain) of many coupled phenomena involved in the hardening process of cementitious materials during the early ages, the most relevant ones for the scope of the present paper being the hydration heat generation, the moisture distribution and their interactions. The input data for that code includes the concrete characterization (mix proportions, type of cement, clinker composition), the environmental conditions (temperature and relative humidity), the structural geometry and the loading. Microphysical information of temperature, hydration ratio, pore structure and moisture transport inside the cementitious materials are computed by DuCOM.

Existing numerical models for predicting moisture fields in cementitious materials at early ages rely on moisture emissivity coefficients varying according to 'a priori' defined laws along time [4–6], to account in a simplified manner for the build-up of the paste microstructure and the subsequent transition from environmentally controlled evaporation to diffusion controlled one. However, for a physically sound modelling, the changes that occur in the evaporation rates from a freshly cast cementitious material should instead be simulated with regards to the evolving pore microstructure, taking as well into account the transition that occurs in the near surface pores from a totally to a partially saturated state.

Based on a literature review and the experiments already documented in the Part I companion paper [1], novel formulations for the moisture boundary conditions, suitable for numerical simulations, are put forward in Sect. 2 of this paper, where regards are also made about the inclusion of the evaporative cooling phenomenon in the computation of heat fields inside cementitious materials during hydration. Section 3 deals with the validation of the proposed models in view of the experimental results documented in the Part I companion paper. In Sect. 4 two numerical sensitivity analyses are described: the first one regarding the relative importance of the parameters involved in the proposed moisture boundary model, and the second one related to the importance of the evaporative cooling phenomenon under varying environmental and curing conditions.

2 Numerical model

2.1 General description

To allow for a proper understanding of how the moisture boundary conditions that will be proposed in Sect. 2.2 affect the curing conditions of cementitious materials, a general description of the DuCOM computation code is presented first. As stated before, this microstructural simulation model accounts for the heat generated by cement hydration and consequent temperature development, as well as for the pore structure formation and internal moisture transport [2, 3].

As far as the heat development in cementitious materials is concerned, the Fourier's law is adopted

$$\rho c \frac{\partial T}{\partial t} = \mathrm{div}(k \nabla T) + H \tag{1}$$

where k is the thermal conductivity, ρc is the heat capacity, T is temperature, t is time and H is the

internal heat generation rate. In DuCOM H is computed upon use of the multi-component model [3, 7], in which the total heat generated by the cement hydration arises from the contribution of the several clinker components involved. Simultaneously with this chemically based computation of the heat generation, a pore structure is computed, allowing for the existence of three classes of pores (interlayer, gel and capillary), whose size distributions evolve during hydration.

In DuCOM, the moisture fields within cementitious materials are calculated according to the following equation for mass balance in porous media [3]

$$\rho_L\left(\sum_i \phi_i \frac{\partial S_i}{\partial P}\right) - \mathrm{div}(k_L \nabla P) + Q = 0 \qquad (2)$$

where ρ_L is the pore water density, ϕ_i is the porosity of each class 'i' of pores (interlayer, gel and capillary), S_i is the degree of saturation of the ith class of pores, k_L is the moisture conductivity (for liquid and vapour), P is the equivalent liquid pore pressure and Q is the sink term (it reflects the internal moisture loss due to water consumption in cement hydration reactions, and the changes in the bulk porosity distribution of the hardened cement-paste matrix). Notice that the outputs of Eq. 1 are spatial distributions of temperature and calculated porosities, which are inputs for the moisture model inherent to Eq. 2. On the other hand, the moisture movements calculated in Eq. 2 affect the availability of water, which in turn largely influences the heat generation rate H in Eq. 1. Therefore, both the heat and moisture models interact.

2.2 New proposal for moisture boundary conditions

Numerical simulation of the moisture interaction between the cementitious materials and the surrounding environment should involve the determination of the moisture fields in both media (i.e. the numerical simulation of the external air/vapour flow and the mass balance inside the cementitious material). Yet, such strategy is practically unfeasible, since it requires an accurate characterization of the environment. Being the aim of the intended numerical analysis to predict the moisture field inside the cementitious material, a simplification is proposed here based on the definition of appropriate moisture boundary conditions using mass transfer coefficients as in Ref. [8].

It has been observed by previous authors [4, 9, 10], and confirmed in the experimental campaign reported in the companion paper [1], that the evaporation from a freshly cast concrete/mortar surface and from a free water surface are identical for a limited time, after which rates of evaporation from concrete/mortar start decreasing. This kind of observation is consistent with the three phases of drying rate of porous media described in the companion paper [1].

The moisture boundary conditions approach of the present research is based on the hypothesis that initially the potential for water evaporation from the surface of a freshly cast (wet) cementitious material can be computed with the same formulas as the ones currently used for a water pan. The subsequent reduction of evaporation rates should therefore be a consequence of the densification of the material pore structure, which inhibits the extent of evaporation, leading to a diffusion controlled evaporation. This effect is simulated with the moisture model of DuCOM, and it depends of many factors such as the water vapour concentration in the atmosphere, the wind speed, the w/c ratio, the geometry of the specimen, the temperature field inside the cementitious material due to the hydration reactions, the age at which the surface is exposed to the environment, the hydration extent, etc. A previous empirical equation had been put forward by Al-Fadhala and Hover [4], to predict the decrease of the rate of moisture loss from a concrete surface when compared to the one from a water pan. Yet, this equation fails to account for the influencing factors that have just been described, and therefore its scope of application is limited. Selih et al. [6] reported experimental research on moisture fields in concrete, as well as numerical simulations where the boundary conditions were simulated as imposed moisture fluxes on the surfaces, based on the measured evolving fluxes from the specimens in their experiments. This kind of approach is not apt for moisture field prediction in arbitrary environmental conditions. The methodology to be presented herein may be considered of general application for predictive purposes.

Bearing in mind that the boundary conditions to be proposed are based on the evaporation from a water surface, three important points are remarked about the current state of knowledge about water evaporation [11]: (i) there is no universal equation for predicting evaporation rates; (ii) the driving potential for evaporation is the difference in vapour pressure between the surface and the environment; (iii) evaporation predictive formulas usually include terms of empirical nature, and even though many attempts have been made up to the present date, there is no analytical definition for it. The evaporation rate equation from a water surface can be displayed in the following format, already presented in the Part I companion paper

$$q_s = E(e_s - e) \tag{3}$$

where E is the moisture emissivity coefficient, e_s is the saturation vapour pressure of water and e is the vapour pressure in the air. Definition of E is not consensual, and many empirical approaches have been put forward [4, 11–15], most of them function of the wind speed. In fact, the applicability of those empirical equations for water evaporation is quite dependent on the exact replication of the original conditions under which they were derived [16]. Yet, a simple procedure can be adopted (in both laboratory and construction sites), and it is proposed here: to characterize the evaporation potential of the testing environment by the use of a simple water pan, exposed to the studied environment (with known temperature and water vapour pressure) and regularly weighted. From the data collected with this simple and reliable test, the moisture emissivity coefficient for water in Eq. 3 can be determined once all the other involved variables are known.

The proposal here made to reproduce the mass transfers that influence the drying induced moisture losses from cementitious materials to the environment is to apply Eq. 3 directly as a boundary condition to the moisture field problem described in Eq. 2. Therefore, it is assumed that the near-surface exposed pores of the cementitious materials can exchange moisture with the environment in accordance to their water vapour pressure (which replaces e_s in Eq. 3), computed on the base of the average pore relative humidity.

However, in real structural applications care should be taken in what regards the coefficients E to be adopted, as due to microclimatic effects they can exhibit great variations in space and time [17].

2.3 Simulation of the evaporative cooling phenomenon

A description of the proposed boundary model for simulation of the effect of evaporative cooling in cementitious materials is made in this section. The basic idea of the model is to calculate the additional heat flux that occurs at the boundaries of the cementitious material as a consequence of the moisture flux. This additional heat flux is computed by a multiplying the moisture flux by the latent heat of vapourization of water (which is a measure of the energy barrier that needs to be overcome for evaporation to be possible). In other words, the described methodology may be explained as: at a given calculation time step, the additional surface heat flux q_{ec} [$\mathrm{Wm^{-2}}$] that occurs at the interface between the material and the environment as a consequence of the moisture evaporative flux q_S [kg $\mathrm{m^{-2}}$ $\mathrm{s^{-1}}$] (as calculated from Eq. 3) can be obtained with the knowledge of the latent heat of vapourization of water h_l [J $\mathrm{kg^{-1}}$] [16]

$$q_{ec} = q_s h_l \tag{4}$$

where [18]

$$h_l = 2500 \times 10^3 - 2500\,(T_S - 273.15) \tag{5}$$

(T_S in Kelvin).

The effect of evaporative cooling is superimposed to the other heat boundary conditions, so that the total heat flux q at the boundary is the sum of the heat fluxes due to convection, irradiation, solar radiation and evaporative cooling [5, 16].

3 Numerical predictions versus experimental results

By using the methodologies described in Sect. 2 of the present paper, numerical simulations of the experiments reported in the companion paper [1] will be presented in order to check the adequacy of

the proposals here made to reproduce the moisture boundary conditions and the evaporative cooling phenomenon in cementitious materials.

3.1 Effects of temperature and relative humidity

The 5 cm diameter and 5 cm tall mortar cylinders referred in Sect. 2.1 of the companion paper were modelled in DuCOM with the mesh depicted in Fig. 1, comprising 3D 8-nodded finite elements (FE). In terms of boundary conditions, three situations occur: on the top exposed surface both moisture and heat transmissions were allowed; in the lateral and bottom form surfaces thermal fluxes were considered, but no moisture exchanges were permitted; in the remaining two surfaces heat and moisture fluxes were prevented. The moisture emissivity coefficient (involved in the novel moisture boundary condition expressed by Eq. 3) for the top surface in each environmental condition was evaluated by following the water evaporation experiment outlined in Sect. 2.2. The obtained values for this coefficient were already presented in Table 3 of the companion paper [1]. Numerical analyses were conducted according to a time integration scheme whose first step had a length of 0.0002 days (approximately 17.3 s), and from then on time steps were successively increased by a factor of 1.05 until the age of 28 days.

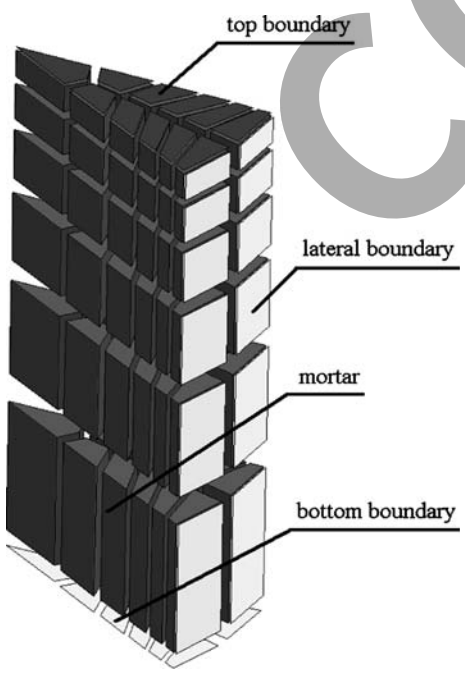

Fig. 1 FE mesh for cylindrical mortar specimens

Predictions from the numerical model for evaluating the influence of temperature T and relative humidity RH on the weight losses are compared to the experimental results in Figs. 2–4. The new proposal for reproducing the moisture boundary conditions appears to have a good performance both for mortars 'H' ($w/c = 0.35$) and 'N' ($w/c = 0.55$): the ascending branch of the weight loss curve is correctly reproduced; both the transition and the diffusion

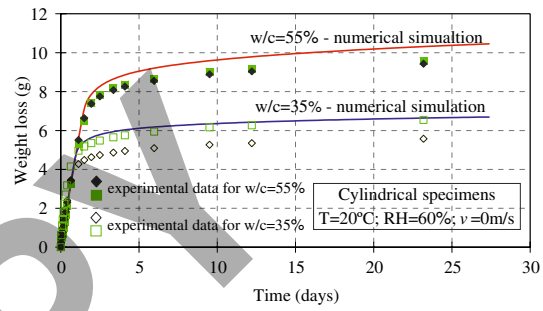

Fig. 2 Weight losses for $T = 20°C$ and RH = 60%

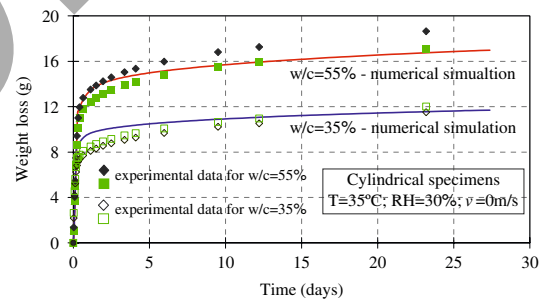

Fig. 3 Weight losses for $T = 35°C$ and RH = 30%

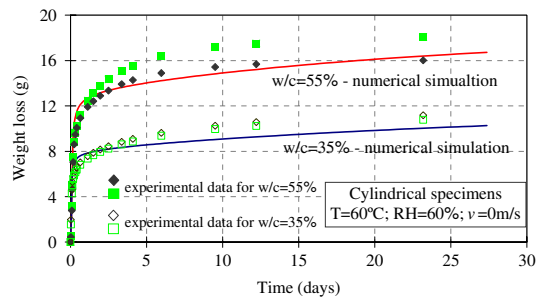

Fig. 4 Weight losses for $T = 60°C$ and RH = 60%

controlled phases (as defined in Fig. 1 of the companion paper) are also fairly reproduced. It is important remark that the agreement of the numerical predictions against the experimental observations is a consequence of an appropriate simulation of the thermal-moisture boundary conditions, as well as of a good prediction of the internal evolution of the pore structure and respective moisture field under arbitrary internal temperature conditions (for further details see Ref. [19]).

In Fig. 5 numerical results regarding the evolution of both the weight loss of the sample with mortar 'N' and the pore relative humidity at depths 0.6, 2.4 and 9.3 mm from the exposed surface are represented for the environmental case of $T = 20^{\circ}C$ and RH = 60%. From Fig. 5 it can be observed that the drop in the rate of moisture loss from the sample approximately coincides with a strong decay of the pore relative humidity in the vicinity of the surface (roughly saying, until 2.4 mm deep).

3.2 Effect of wind

The prismatic 7.3 × 5.1 × 3.0 cm mortar specimens mentioned in Sect. 2.2 of the companion paper were modelled in DuCOM with 3 D 8-nodded FE according to the FE model geometry of 1/4 of the specimen depicted in Fig. 6. The adopted boundary conditions are: in the top exposed surface heat and moisture fluxes are allowed, while in both the lateral and bottom boundaries (corresponding to contacts with the form surfaces) only thermal fluxes are allowed. In symmetry planes all fuxes were prevented.

To numerically simulate the tests concerned with the influence of wind on the weight losses of specimens 'H' and 'N', and reported in the companion paper [1] for the wind speeds $v = 0$, 1.8, 3.3 and 4.2, the experimentally determined values of E (according to Eq. 3) for water specimens with the same exposed surface are listed in Table 1. The time steps and the total period of analysis for the present numerical simulations are the same as in the previous Section.

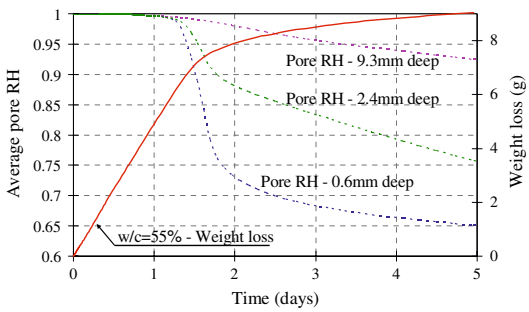

Fig. 5 Evolution of pore RH and weigh loss for $T = 20^{\circ}C$ and RH = 60%—numerical simulation

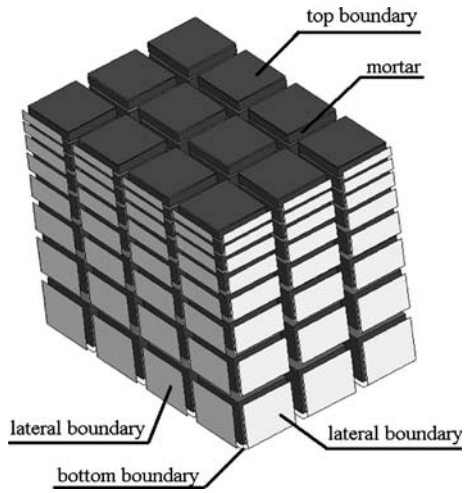

Fig. 6 FE mesh for the prismatic mortar specimens

Table 1 Moisture emissivity coefficients (prismatic specimens)

v (m/s)	E (kg m^{-2} s^{-1} Pa^{-1})
0	2.00E-08
1.8	4.92E-08
3.3	7.66E-08
4.2	9.09E-08

The numerical predictions from the performed analyses may be compared with the experimentally measured weight losses in Figs. 7–10: a quite satisfactory agreement is observed, which once more points to the validity of the adopted numerical model and moisture boundary conditions approach.

At this point, and by just performing numerical simulations, it is interesting to check the overall effect of variable wind speed on the evolution of the weight losses from the samples. Figure 11 reproduces the predicted weight losses for the tested wind speeds and for the two studied mortars: it becomes clear that the linear ascending branch of the weight loss, associated to the environmentally controlled evaporation, has the same slope for both mortars, provided the same wind speed is considered. The transition for

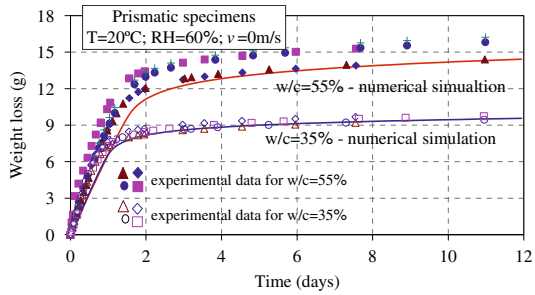

Fig. 7 Weight losses for v = 0 m/s

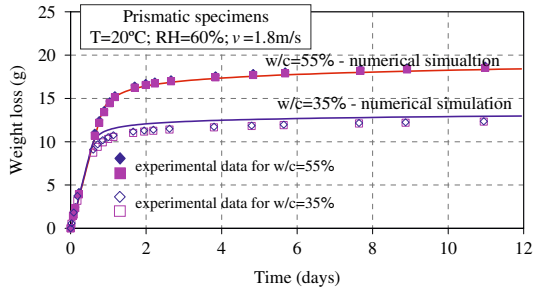

Fig. 8 Weight losses for v = 1.8 m/s

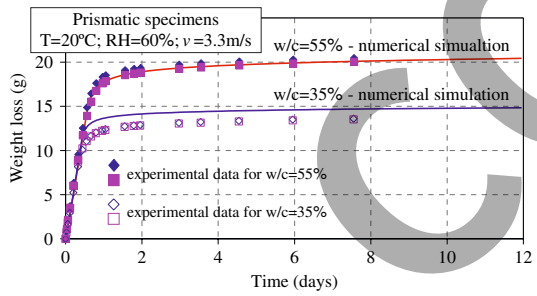

Fig. 9 Weight losses for v = 3.3 m/s

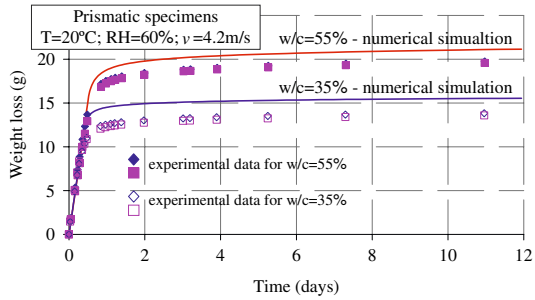

Fig. 10 Weight losses for v = 4.2 m/s

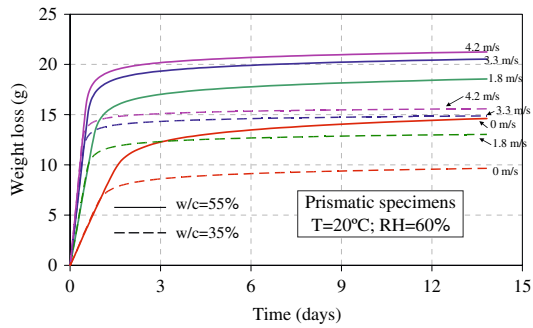

Fig. 11 Weight losses under variable wind speed—numerical simulation

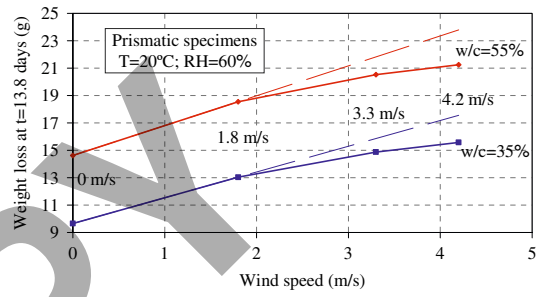

Fig. 12 Weight loss at t = 13.8 days as a function of wind speed—numerical simulation

diffusion controlled moisture loss occurs sooner for w/c = 0.35 than for w/c = 0.55, and the final weight losses for the 'H' mortar are lower than for the 'N' one. Dependency of the final value of the weight loss on v is depicted in Fig. 12: it is interesting to note that the ratio between the weight losses in the two mortars is almost constant, with an average value of 1.42 (which fairly resembles the quotient between the w/c ratios 55/35 = 1.57). In addition, the plotted dashed lines represent the expectable weight losses if the relationship with v was linear: it can be concluded that as v increases its effect on the water removal from mortar reduces.

3.3 Effect of age of sealing removal

In the numerical analyses of this Section, where the influence of the age of sealing removal on the weight losses of the mortar samples will be checked, the mesh geometry, boundaries, time steps and material characteristics are the same as the ones mentioned in the previous Section, except for the age at which the moisture boundary conditions are activated.

The numerical predictions, as well as the experimental measurements of the weight losses in the cases of sealing removal at 1, 3 and 7 days are plotted in Figs. 13–15. From observation of Fig. 13 it can be noticed that the numerical simulations clearly over predict the final weight losses as a consequence of having longer ascending branches than the ones verified in the experiments. This difference may be in part attributed to the experimental procedure: upon sealing removal at 1 day the use of a moist cloth to remove drops of what appeared to be bleed water may have resulted in an excessive removal of surface moisture. Yet, the numerical predictions for sealing removal at the ages of 3 and 7 days seem to be reasonably good when compared to the experimental results (Figs. 14, 15).

For an overall comprehension of the influences on the weight losses due to variable wind speeds and ages of sealing removal, the numerical results depicted in Fig. 16 are invoked: it is quite evident that the effect of wind is much stronger for earlier ages of sealing removal, becoming almost negligible for later ages; moisture losses clearly diminish with later sealing removal.

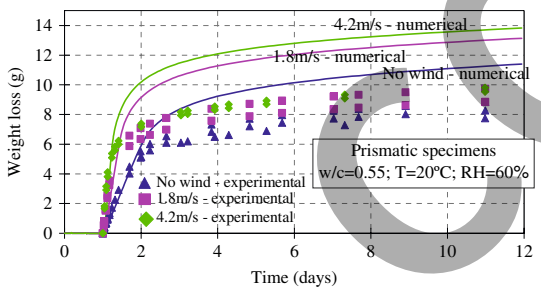

Fig. 13 Weight losses for a sealing removal at the age of 1 day

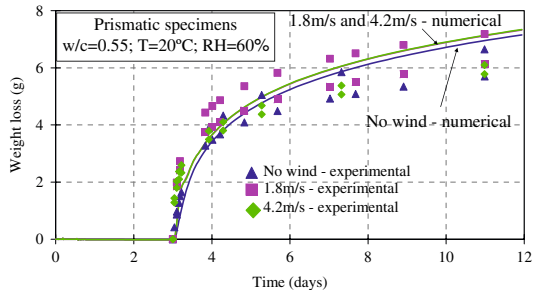

Fig. 14 Weight losses for a sealing removal at the age of 3 days

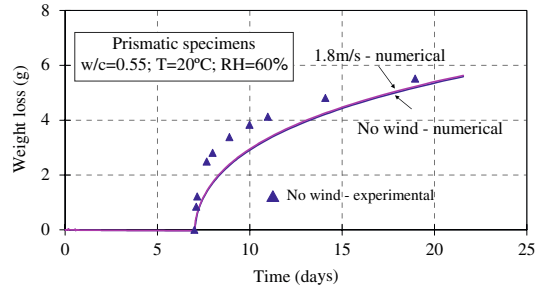

Fig. 15 Weight losses for a sealing removal at the age of 7 days

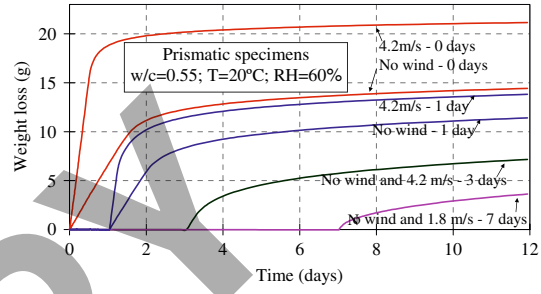

Fig. 16 Weight losses as a function of wind speed and age of sealing removal—numerical simulation

3.4 Effect of evaporative cooling

The numerical strategy that was used to simulate the evaporative cooling experiment reported in the companion paper [1] is essentially the same as adopted in the previous two Sections, except that the environmental conditions are now $T = 36.4°C$ and RH = 30%. In accordance to the values measured in water specimens under these environmental conditions the value of 5.0×10^{-8} kg m^2 s^{-1} Pa^{-1} was adopted for E. In regard to heat convection coefficients, firstly a value of 5 W/m^2 K was adopted on all the specimen's surfaces to account for the heat shielding effect provided by the sealing material; upon sealing removal the convection/radiation coefficient on the exposed surface was increased to 11.6 W/m^2 K, to reproduce the direct contact with the environment. The numerical predictions will be compared to the experimental results in terms of the evolutions of both the weight loss (Fig. 17) and the temperature evolution (Fig. 18). Figure 17 demonstrates that the numerical model predicts fairly well the moisture fluxes from the specimen, which is a good starting point for the evaporative cooling

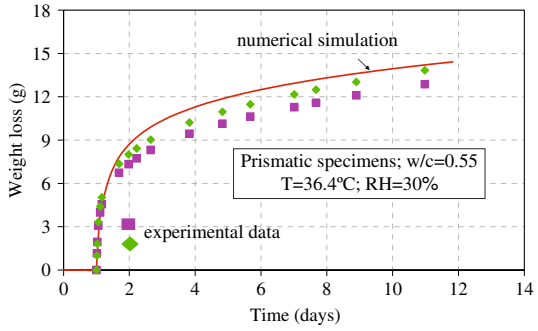

Fig. 17 Weight loss during the evaporative cooling test

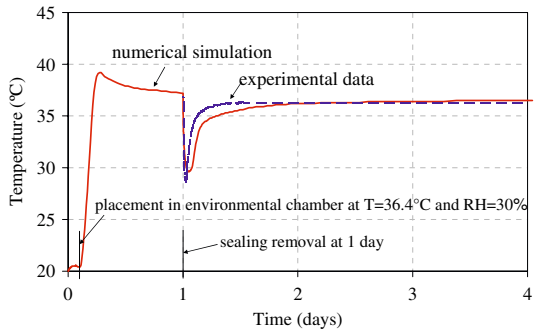

Fig. 18 Temperature evolution during the evaporative cooling test

prediction, as such fluxes are used for estimation of the heat removal (see Eq. 4). The temperature evolution in the specimen is depicted in Fig. 18, where the experimental results are only plotted immediately after exposure at 1 day, while the numerical results are plotted since casting at 20°C and later placement in the environmental chamber at 36.4°C. The temperature drop prediction upon sealing removal matched quite well the measured one. Yet, the return of the mortar temperature to equilibrium with the environmental one was slightly slower in the numerical model than it actually happened in the experiment.

4 Sensitivity analyses

4.1 Overview

Taking advantage of the numerical framework to simulate the heat/moisture fields in cementitious materials at early ages, two sensitivity analyses concerning the influence of boundary conditions will be presented.

4.2 Influence of E and of the driving potential

This first sensitivity analysis aims to clarify the differences in the behaviour of two identical mortar specimens when each of them is subjected to dissimilar environmental conditions that nonetheless yield matching moisture fluxes in water pans: one moist environment with wind conditions and another environment with less humidity and stagnant air conditions. The reasons for a different drying behaviour of the mortars are clarified.

Considering the same geometry of the mortar specimens of Sect. 3.3, and an age of sealing removal of 3 days, two rather different environmental conditions were considered, listed in Table 2 as Conditions 1 and 2. In both situations the environmental temperature is 20°C, but with different RH (respectively 60% and 30% for Conditions 1 and 2). In Condition 1, a wind speed of 0.88 m/s was considered, while in Condition 2 $v = 0$ m/s. The environmental and the surface vapour pressures were calculated by the use of Eq. 3 of the companion paper [1], considering the multiplication by the relevant relative humidity (note that in the wet mortar surface, a RH = 100% was considered at the beginning of exposure). Considering that Eq. 2 in the companion paper is applicable in the hypothetical wind conditions of these tests, the computed moisture emissivity coefficients are respectively 3.83×10^{-8} kg m^2 s^{-1} Pa^{-1} and 2.19×10^{-8} kgm^2 s^{-1} Pa^{-1} for Conditions 1 and 2. Using Eq. 3 the calculated moisture fluxes in the boundaries for both situations are virtually the same, that is, $\sim 3.58 \times 10^{-5}$ kg m^2 s^{-1}, which means that two water pans left in these two environmental conditions would have the same moisture losses. In the case of mortar the situation is not quite like that: considering two mortar specimens under the mentioned environmental conditions, and with the top sealing removed at the age of 3 days, the moisture loss rates immediately after formwork removal would be identical (as in the case of water pans). Yet, as soon

Table 2 Environmental conditions for the sensitivity analyses

Condition	T (°C)	RH (%)	e (Pa)	e_s (Pa)	v (m/s)
1	20	60	1,404	2,340	0.88
2	20	30	702	2,340	0.00

as the surface humidity starts dropping bellow the total saturation, the moisture boundary flux for Condition 2 (RH = 30%) will take place at higher rates than for Condition 1 (RH = 60%). For example, when the surface humidity becomes 90% the calculated boundary fluxes would be

$$q_{\text{Cond1}} = 3.83 \times 10^{-8}(0.9 \times 2340 - 0.6 \times 2340) = 2.69 \times 10^{-5}\,\text{kg m}^{-2}\,\text{s}^{-1}$$

$$q_{\text{Cond2}} = 2.19 \times 10^{-8}(0.9 \times 2340 - 0.3 \times 2340) = 3.07 \times 10^{-5}\text{kgm}^{-2}\text{s}^{1}$$

which means that the boundary fluxes would have become 75.1% and 85.5% of their original values for Conditions 1 and 2. As the surface moisture content decreases, this difference in the moisture loss rates increases. This reasoning can be consubstantiated by the observation of the numerical results for both conditions in terms of the moisture fluxes and weight losses depicted in Fig. 19. In fact, it is noticeable that the moisture flux starts decreasing almost immediately after sealing removal, but the decrease in this rate is stronger for Condition 1 (RH = 60%) than for Condition 2 (RH = 30%), particularly during the first day after exposure. In spite of these differences in the rates of moisture loss, it is only after the end of the first day of exposure that the total weight loss differences between the two conditions become evident. Also, attention is drawn again to Fig. 19 where it can be confirmed that the final weight loss for Condition 2 is clearly higher than the one for Condition 1. In Fig. 20, which depicts the evolution of RH in the pore structure near the exposed surface,

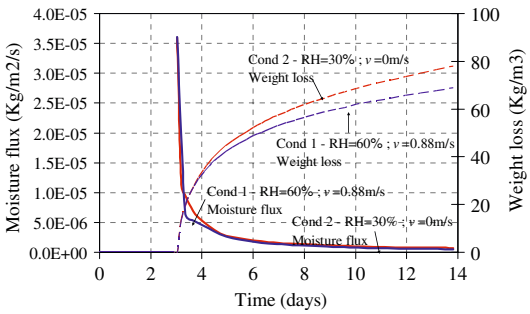

Fig. 19 Moisture flux and weight loss for Conditions 1 and 2—numerical simulation

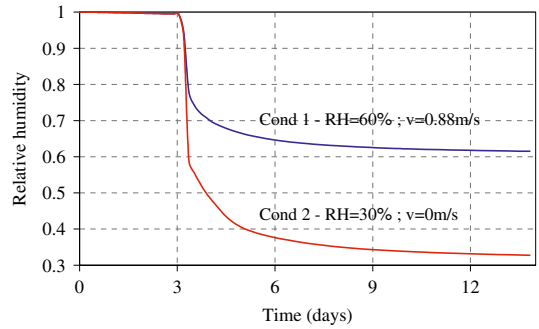

Fig. 20 Evolution of near surface (at 0.2 mm depth) relative humidity for Conditions 1 and 2—numerical simulation

it can be seen that the moisture content drop is faster for Condition 2 than for Condition 1, as a consequence of the higher moisture loss rates. In addition, it can be seen that after some time (which is different for each situation), both surfaces will be in quasi-equilibrium with the respective environmental conditions: at 14 days the surface RH of specimen 1 is very near 60%, and for specimen 2 the surface RH $\approx$ 30%. Nevertheless, even at the end of the analysis (t = 14 days), the rates of water evaporation in Condition 2 are higher than the ones for Condition 1. The reason for this is relatively easy to understand: at this moment the loss of water from the mortar is no longer controlled only by environmental conditions, since it has become diffusion controlled. Yet, the moisture gradients between the saturated mortar cores and the surface (in quasi-equilibrium with the environment) are higher for the case where the environment has RH = 30%, and therefore the internal moisture transport will be faster.

As a conclusion, this sensitivity analysis puts into evidence the preponderance of the driving potential (i.e. the vapour pressure difference) over the moisture emissivity coefficient in the process of concrete drying.

4.3 Influence of age of sealing removal and temperature on evaporative cooling

Considering the situation as described in Sect. 3.4 (evaporative cooling test in a prismatic specimen under T = 36.4°C and RH = 30%), two further scenarios were numerically analyzed: sealing removal at the ages of 3 and 7 days. The comparative plots of both the moisture losses and the temperature

evolutions are depicted in Fig. 21. As expected, the later the sealing removal occurs, the lower becomes the moisture loss rate and the evaporative cooling temperature drop (~7.6°C for a sealing removal at the age of 1 day; ~3.5°C at the age of 3 days and ~2.7°C at the age of 7 days). Another issue that is dealt with in this sensitivity analysis is the numerical prediction of the evaporative cooling that occurs on a specimen at the age of exposure of 1 day, under the conditions as described in Sect. 3.4, or when subjected to a lower environmental temperature, such as $T = 20°C$, and with rather different RH of 30% or 60%. The results of these analyses in terms of both moisture losses and temperature evolutions are depicted in Fig. 22: due to lower environmental temperatures, the vapour pressure difference between the paste and the environment is smaller for $T = 20°C$ than for $T = 36.4°C$. Consequently the moisture losses vary in accordance, and therefore the evaporative cooling temperature drop becomes attenuated: its magnitude is about 7.5°C for $T = 36.4°C$ and RH = 30%, 4.0°C for $T = 20.0°C$ and RH = 30% and 2.3°C for $T = 20.0°C$ and RH = 60%.

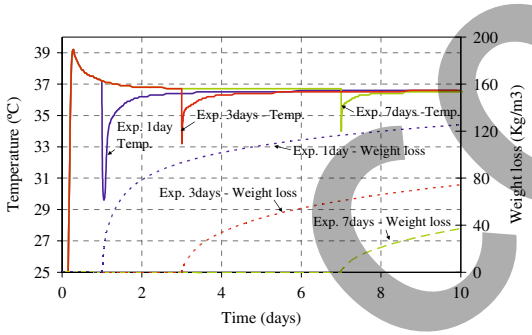

Fig. 21 Evaporative cooling effect for sealing removals at the ages of 1, 3 and 7 days—numerical simulation

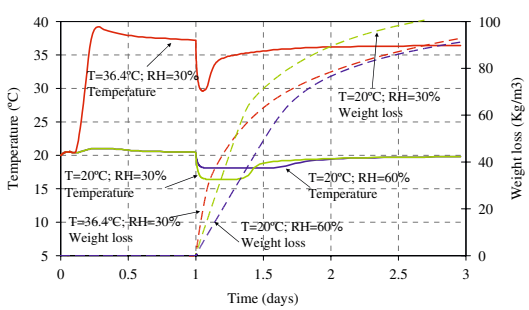

Fig. 22 Evaporative cooling tests at 20°C and 36.4°C, for a sealing removal at the age of 1 day—numerical simulations

Finally one last issue is dealt with in what regards to the evaporative cooling: the effect of the concrete surface being hotter than the environment upon formwork removal. For this concern, a 40 cm thick concrete wall was considered. No specific details are given in this paper about the analysis, except that the environment is characterized by T = 20°C and RH = 60%; a highly insulating formwork is considered and it is considered to be removed at the age of 1 day (for more specific details on this calculation, see Ref. [16]). The calculated temperature evolution for the surface of the wall with and without the consideration of the evaporative cooling effect is depicted in Fig. 23. Without consideration of the evaporative cooling, the surface temperature rises from 20°C (environmental temperature) to a peak value of about 56°C at 16 h of age. After that a decreasing period begins, which is relatively stable until the age of 1 day, when the insulating formwork is removed. As a result of a strong change in the thermal boundary conditions, the temperature drop becomes steeper and converges to almost 20°C at the age of 3 days. If the evaporative cooling phenomenon is considered, right after casting there is a very strong sudden moisture loss due to the concrete temperature being much higher than the environment which causes a large and sudden drop in the surface temperature (about 9°C). Afterwards there is a slight heating of the concrete surface caused by the heat stored in the core. Eventually the temperature evolution becomes quite similar to the one that would happen if no evaporative cooling happened. Therefore, an important warning for concrete construction practice arises: any formwork removal while concrete is hotter than the environment may result in an

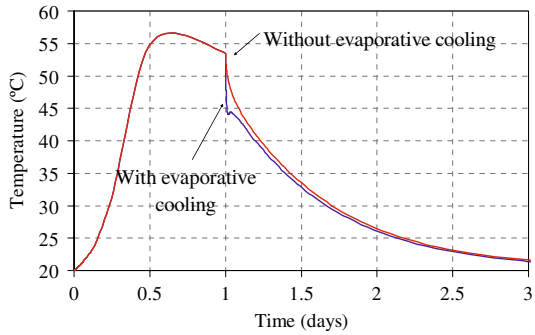

Fig. 23 Temperature evolution in the surface of a 40 cm thick wall with and without evaporative cooling

increased risk of surface cracking due to the evaporative cooling effect.

5 Conclusions

The capability of predicting moisture losses from cementitious materials at early ages is a quite important issue for a durability oriented numerical analysis of a concrete structure. On one hand, the water shortage due to evaporation in near surface areas can lead to a deceleration of the cement hydration reactions, consequently inducing coarser pore structures, and thus posing durability problems. On the other hand, the moisture losses may be responsible for tensile stresses on the surface (due to drying shrinkage and/or evaporative cooling), with possible resulting surface cracks that are detrimental from both aesthetical and durability points of view. In the present paper a formulation was proposed to reproduce numerically the boundary conditions between cementitious materials and the environment, applicable for predicting early-age drying induced moisture losses under arbitrary conditions of temperature, relative humidity and wind speed. It expresses the evaporation at the boundary as linearly dependent on the water vapour pressure difference between the material exposed surface and the environment, and it uses a moisture emissivity coefficient that accounts for the influence of the wind speed; this coefficient can be easily determined by monitoring weight losses from water pans placed on the environmental conditions under study. The computational code used in this research (DuCOM) for determining the thermal and moisture fields on mortar or concrete specimens accounts for the simultaneous densification of the pore structure and the moisture shortage in near surface areas, due to both autogenous water consumption and evaporation to the environment. So, the implementation on that code of the novel moisture boundary conditions here presented allows the evaporation from freshly cast cementitious materials to be consistently reproduced, including its deceleration as the hydration reaction progresses. In addition, a heat/moisture boundary formulation was proposed to account for the evaporative cooling phenomenon that occurs just after formwork removal. It basically consists in using the computed evaporative moisture losses to calculate the heat removal from the mortar surface upon knowledge of the latent heat of evaporation of water. The computed heat removal is thereafter prescribed as a thermal flux at the boundaries of the DuCOM finite element mesh, and so an interaction between the moisture and temperature fields is considered on the numerical simulation of the evaporative cooling.

Adequacy of the new boundary conditions was checked by reproducing numerically the experimental results for cementitious materials reported in the Part I companion paper (Part I). The agreement between the numerical predictions and the experimental results was fairly good in almost all the situations.

Two sensitivity analyses were finally presented. In the first one, concerning the relative importance of the wind speed and the driving potential (i.e. the water vapour pressure difference between the exposed surface and the environment), it was concluded that the driving potential in long-term water losses from cementitious materials is the dominant issue, being relevant even when the evaporation is diffusion controlled (unlike wind, whose influence becomes almost negligible). In the second sensitivity analysis relevance of the evaporative cooling phenomenon was numerically investigated under several environmental conditions and ages of exposure, leading to the conclusion that for real concrete structures the temperature drop due to evaporative cooling becomes specially relevant when formwork is removed while concrete is still hotter than the environment.

Acknowledgement Financial support from the Portuguese Foundation for Science and Technology, through the PhD grant provided to the first author (SFRH/BD/13137/2003) and the Research Project POCI/ECM/56458/2004, is gratefully acknowledged.

References

1. Azenha M, Maekawa K, Ishida T, Faria R (2007) Drying induced moisture losses from mortar to the environment - Part I–experimental research. Mater Struct DOI:10.1617/s11527-007-9244-y
2. Maekawa K, Ishida T, Kishi T (2003) Multi-scale modeling of concrete performance. Integrated material and structural mechanics. J Adv Concrete Technol 1(2):91–126
3. Maekawa K, Chaube R, Kishi T (1999) Modelling of concrete performance. E&FN SPON 308
4. Al-Fadhala M, Hover K (2001) Rapid evaporation from freshly cast concrete and the Gulf environment. Constr Building Mat 15:1–7

5. Schindler A, Ruiz J, Rasmussen R, Chang G, Wathne L (2003) Concrete pavement temperature prediction and case studies with the FHWA HIPERPAV models. Cement Concrete Compos 26(5):463–471
6. Selih J, Sousa A, Bremner T (1996) Moisture transport in initially fully saturated concrete during drying. Transp Porous Media 24:81–106
7. Kishi T, Maekawa K (1995) Multi-component model for hydration heating of portland cement. Concrete lib JSCE–Jap Soc Civil Eng 28:97–115
8. Masmoudi W, Prat M (1991) Heat and mass transfer between a porous medium and a parallel external flow. Application to drying capillary of porous materials. Int J Heat Mass Transfer 34(8):1975–1989
9. Uno PJ (1998) Plastic shrinkage cracking and evaporation formulas. ACI Mater J 95(4):365–375
10. ACI (2001) Guide to curing concrete. ACI Committee Reports, A. C. Institute, ed.
11. Jones F (1992) Evaporation of water with emphasis on applications and measurements. Lewis Publication, Michigan
12. Marek K, J S (2000) Analysis of the evaporation coefficient and the condensation coefficient of water. Int J Heat Mass Transfer (44):39–53
13. Bansal P, Xie G (1998) A unified empirical correlation for evaporation of water at low air velocities. Int Comm Heat Mass Transfer 25(2):183–190
14. Pauken M (1999) An experimental investigation of combined turbulent free and forced evaporation. Exp Thermal Fluid Sci. (18):334–340
15. Eames I, Marr N, Sabir H (1997) The evaporation coefficient of water: a review. Int J Heat Mass Transfer 40(12):2963–2973
16. Azenha M, Maekawa K, Ishida T, Faria R (2005) Heat and moisture transfer between concrete and the environment. LABEST–internal reports
17. Nilsson L-O (1996) Interaction between microclimate and concrete–A prerequisite for deterioration. Const Building Mater 10(5 SPEC. ISS.):301–308
18. Chuntranuluck S, Wells C, Cleland A (1998) Prediction of chilling times of foods in situations where evaporative cooling is significant–Part 1 method development. J Food Eng 37:111–125
19. Ishida T, Maekawa K, Kishi T (2007) Enhanced modeling of moisture equilibrium and transport in cementitious materials under arbitrary temperature and relative humidity history. Cem. Conc. Res 37(4):565–578